Applied Catalysis B: Environmental 202 (2017) 147–155

Contents lists available at ScienceDirect

Applied Catalysis B: Environmental

journal homepage: www.elsevier.com/locate/apcatb

Assessment of mechanisms for enhanced performance of TiO_2/YAG:Yb^{+3},Er^{+3} composite photocatalysts for organic degradation

Jon W. Pickering, Venkat R. Bhethanabotla*, John N. Kuhn*

University of South Florida, Tampa, FL 33620, United States

ARTICLE INFO

Article history:
Received 5 January 2016
Received in revised form 1 August 2016
Accepted 2 September 2016
Available online 6 September 2016

Keywords:
Heterogeneous photocatalysis
Upconversion
Rare earth metal
Titania
YAG host

ABSTRACT

Wastewater remediation is a key component to a sustainable water management program and the use of photo-activated catalysis has emerged as a promising advanced oxidative process for the decomposition of organic contaminants to innocuous products. Although the process is feasible using UV photons, only ~5% of solar insolation is comprised of UV photons and few advances have been made to improve upon commercial TiO_2 (i.e., P25). Here, composite catalysts containing both an upconversion phase (Yb^{+3}/Er^{+3}/Y-Al garnet or YAG host) and a photocatalyst (TiO_2) are assessed for enhancing the photocatalytic activity of TiO_2 for organic degradation using simulated insolation. Samples of the upconverting phosphor (YAG host) were prepared utilizing the Pechini method with varying molar concentration of Yb^{+3} ions [0%, 10%, 15%, or 20%] and a constant concentration of Er^{+3} ions [2%]. The composite materials were then obtained via calcination of the various YAG:Yb^{+3},Er^{+3} samples with titania at molar concentrations of [10%, 15%, or 20%]. Structures and properties of the upconverting phosphors and composite materials were verified with characterization analyses including X-ray diffraction, diffuse reflectance spectroscopy, transmission electron microscopy, and photoluminescence spectroscopy. For rose bengal degradation in a batch slurry reaction using a simulated 'daylight' spectrum as the irradiation source, results indicated that a mixed phased, Y-Al oxide doped with 2 mol% Er^{+3} and 15 mol% Yb^{+3} with 10 mol% doped YAG/balance TiO_2 composite yielded a 42% higher rate constant and apparent quantum yield than TiO_2 alone. Additional kinetic studies with portions of the solar spectrum (i.e., UV bulbs or UV or IR LEDs) were conducted to further probe the effect of photon energies and suggested that rate and apparent quantum yield enhancements were largely attributed to increased amounts of organic adsorption and close proximity between phases, which coincided with the presence of the monoclinic phase (not cubic) of the Y-Al oxide structure. Upconversion and decreased charge carrier recombination rates were deemed to provide minimal contribution to these enhancements.

1. Introduction

As industrialization continues around the globe, an increase in water pollution has been realized around the world. Coupling this environmental issue with the growing decline in conventional energy resources suggests that advancing pollution mitigation strategies in an eco-friendly and energy efficient manner is crucial to creating a sustainable water management program. Heterogeneous photocatalysis utilizing TiO_2 as the semiconductor and solar radiation as the energy source has risen in popularity over the past decades as a promising advanced oxidation process (AOP) for wastewater remediation [1,2]. Improving the efficiency at which the sun's energy is used has been addressed in a variety of doping techniques (mainly of TiO_2) involving dyes [3], transition metals [4], metallic nanoparticles [5], other semiconductors [6,7], and rare earth ions (RE^{+3}) [7–10]. From these various techniques, the use of RE^{+3} offers potential for a unique mode of enhancement due to their *f* and *d* orbitals, which allow for the generation of high energy photons from multiple low energy (i.e., visible (Vis) and infrared (IR) wavelength range) absorbed photons via an anti-Stokes process named upconversion luminescence (UCL) [11,12]. The high energy photons are then able to produce separated electron-hole pairs within the photocatalytic semiconductors and provide an avenue to widen the photon energies that contribute to the generation of charge carriers and thus the catalysis. The existence of the UCL-induced photocatalysis has been verified by using low energy photons (with too low of energy to generate significant amounts of

* Corresponding authors at: Department of Chemical & Biomedical Engineering, University of South Florida, Tampa, FL 33620, United States.
E-mail addresses: bhethana@usf.edu (V.R. Bhethanabotla), jnkuhn@usf.edu (J.N. Kuhn).

http://dx.doi.org/10.1016/j.apcatb.2016.09.007
0926-3373/

charge carriers in the semiconductors) and demonstrating the reaction only occurs (or occurs much faster) when the rare earth ions are present and with corresponding optical characterization [9,13–15]. However, a recent study [9] has also reported an enhancement in the photocatalytic performance for rare earth ion doping for TiO_2 even when only UV photons were used. Additional mechanisms would have to exist for this behavior to occur.

As a result, a dual enhancement mechanism [9,10,16] has been proposed in which doping with rare earth metals yields both UCL behavior and depressed electron-hole recombination rates via charge trapping. While both phenomena may be occurring, it is difficult to assess the contribution of each. Beyond these two explanations, it is also plausible for the doping to influence the surface sites, adsorbate strengths, and specific surface area, alter the band gap and shift the positions of the band edges (if doping occurs in the semiconductor phase), and/or provide a secondary phase for charge transfer (if doping occurs in a separate host phase). Enhancements compared to TiO2 have also been reported for rare earth ion composite in which the rare earth ion (Cerium) is not capable for upconversion [7]. As all of these respective contributions may vary with material composition, light irradiation, and the specific reaction and its conditions, significant efforts are needed develop a deep understanding of the structure-function relations of rare earth ion doping of semiconductor photocatalysts.

As just described, studies have recently emerged which provide insights into the enhancements and associated mechanisms of rare earth ion doping on semiconductor photocatalysis under solar radiation. The overall goal of this effort is continue these assessments by evaluating the photocatalytic degradation of a model organic pollutant using a series of composite catalysts containing a semiconductor photocatalyst (i.e., P25 TiO_2) and a rare earth ion containing phase (yttria aluminum garnet or YAG doped with Er and Yb denoted as YAG:Yb,Er). The specific goals are to determine the photocatalytic enhancements of the YAG:RE^{+3} to TiO_2 and the Er:Yb ratios under various irradiation sources (i.e., simulated solar, IR, and UV), which is anticipated to provide insights into the underlying physics and chemistry involved compared to the semiconductor photocatalyst control experiments. Although many of the recent studies directly embedded the RE^{+3} into the semiconductor photocatalyst [8–10,14,16–18], the use of composite catalysts separating the phases of the RE^{+3} and semiconductor photocatalyst has also been examined [13,15,19–21]. This approach was selected to help minimize the many possible effects of embedding the RE^{+3} ions into the semiconductor phase, which include shifting band edge positions and band gaps (even if minor [9]) and changing carrier recombination rates [9,10,13], and the RE^{+3} should be able to be more easily accommodated into trivalent-based lattice of which many common semiconductor photocatalysts (e.g., TiO_2) are not. YAG was selected as the RE^{+3} host phase for these arguments and because of its stability and relatively high surface area (~50 m^2/g for similar synthesis [22]), when compared to other commonly used host materials [11,22–24]. This additional surface area may provide increased organic adsorption near the photocatalyst, reducing diffusion lengths for hydroxyl radicals to adsorbed organics. Er^{+3} was selected as the primary RE^{+3}, as it has a comparatively high UCL efficiency [11], best suited for high energy photon generation via UCL [24–26], and is the most common RE^{+3} in literature studies [8–10,13,14,16–18,20,21,27–30]. To limit the parameters in current study, the amount of Er in the YAG host phase was held constant at 2 mol%. This value is common in the literature studies regardless of the specific host phase [8–10,13,14,16–18,20,21,27–30] with high (>5% mol) amounts leading to quenching [28] and the highest optimal amount being 4 mol% [17]. Yb^{+3} was chosen as the RE^{+3} sensitizing agent in combination with Er as this combination is the amount most commonly examined for dual RE^{+3} combinations and Yb^{+3} contains optical activity in the IR [10,13,25,27,29,30], where ~40% of the photons in the solar spectrum range exist. A wide range of Yb^{+3} amounts (0–20 mol% in YAG phase) were investigated herein, as the ratios examined in the literature vary (e.g., 2%Er:4%Yb [29], 1%Er: 0–2% Yb with 1.5 optimal [30], 2%Er:5%Yb [27], 1%Er:1%Yb [13] and 0–2%Er: 0–10% Yb with 0%Er:1%Yb optimal [10]) and the Yb^{+3}:Er^{+3} ratio is likely important, as well as the irradiation source, host phase, and the specific reaction and conditions. Further studies are needed to probe the reasons for these optimal ratios and assess the opportunities for UCL in photocatalytic studies.

The series of composite catalysts just described (TiO_2/YAG:Er,Yb with varying TiO_2:YAG and Er:Yb ratios) were examined for photocatalytic degradation of rose bengal dye (RB) with simulated solar insolation and separate control experiments with UV and IR photons. Control studies were performed to better understand the contributions of the various enhancement mechanisms such as suppressed electron-hole pair recombination rates, improved pollutant adsorption near the photocatalyst's surface, and the generation of new photons via UCL. The photocatalytic degradation of RB was used as a model reaction in all studies due to extensive reports that RB degradation largely follows the hydroxyl attack mechanism as it is neutral in nature [31–33]. The absence of a positive or negative charge, like the ones found on methylene blue and methyl orange, minimizes the probability of redox reactions directly with the charge carriers. From this study, experimental findings should be able to be extended to applications in which solar radiation is indeed used as an energy source and the contributions of the various enhancement mechanisms should be gauged.

2. Experimental section

2.1. Synthesis of YAG:RE^{+3} upconverting phosphors (UPs)

The YAG:RE^{+3} UPs were synthesized following a method similar to that which was previously reported by Hassanzadeh-Tabrizi [34]. $Y(NO_3)_3{\cdot}6H_2O$ (Sigma-Aldrich, 99.8%), $Al(NO_3)_3{\cdot}9H_2O$ (Alfa Aesar, ACS 98–102%), $Er(NO_3)_3{\cdot}5H_2O$ (Sigma-Aldrich, 99.9%) and $Yb(NO_3)_3{\cdot}5H_2O$ (Sigma-Aldrich, 99.9%) were used as the source of cations. Appropriate amounts of the nitrate salts were dissolved in 80 mL of ultrapure water (Millipore Direct-Q UV3, >18 MΩ*cm) followed by citric acid (CA; Sigma-Aldrich, 99.5%) and then ethylene glycol (EG; Sigma-Aldrich, 99%) at a CA:EG molar ratio of 2:1. The solutions were then introduced into a pre-heated oil bath and were continuously stirred at 80 °C in order to dehydrate the samples and accelerate the polyesterification process. The clear gels were then placed in an oven at 100 °C for 24 h. After which, the obtained aerogels were ground with a mortar and pestle and then calcined at 1000 °C for 3 h.

2.2. Preparation of TiO_2/YAG:RE^{+3} composites

The resulting powders were then combined with AEROXIDE® TiO_2 P25 (Nippon Aerosil, 99.5%) by thoroughly mixing the two compounds via mortar and pestle and 1-propanol (Sigma-Aldrich, 99.9%) followed by a further calcination treatment at 500 °C for 3 h. These samples will be named TiO_2/YAG:RE^{+3} and will be distinguishable by the varying YAG:RE^{+3} and Yb^{+3} molar concentrations, which represent amounts of the total YAG phase in the sample and the amount of Yb in the YAG phase, respectively. Any sample prepared with Er contains 2 mol% Er in the YAG phase.

2.3. Preparation of TiO_2/YAG:RE^{+3} composite films

On a microscope slide, a layer of TiO_2/YAG:RE^{+3} composite was deposited via the doctor blade method. The composite slurry for the doctor blade method was prepared by thoroughly mixing 0.4 g

TiO_2/YAG:RE^{+3}, 0.75 mL water and 0.18 mL ethanol using a mortar and pestle. The film depth was controlled by applying strips of packing tape to either side of the microscope slide, creating a sub mm thick trench to which the paste was evenly spread. The layered substrate was then subjected to air drying on a mechanical shaking table for 30 min to avoid cracking followed by 30 min in an oven at 100 °C.

2.4. Material characterization

X-Ray diffraction (XRD) patterns were obtained using a Bruker, D8 Advance X-ray diffractometer. Diffraction patterns were recorded from 2θ = 15–70° with Cu Kα radiation (λ = 1.5406 Å) for phase analysis and determination of unit cell parameters. Chemical compositions were determined by energy dispersive spectroscopy (EDS) using a Zeiss, EVO 50 scanning electron microscope (SEM) and AZtec analysis software. All measurements were obtained with a backscatter electron detector. Transmission electron microscopy (TEM) was performed with a Philips, FEI Morgagni microscope (M268) to observe and compare the microstructures of the obtained powders. The samples were prepared by dispersing the powders in ethanol via sonication and then vacuum drying a droplet on copper grids. Diffuse reflectance spectroscopy (DRS) was conducted with a Jasco, V-670 Spectrophotometer in order to detect the regions within the Vis and IR spectra that the RE^{+3} are optically active and to obtain the band gap. The powders were analyzed from 350 to 1200 nm using a spectralon reference sample. Photoluminescence spectroscopy (PL) was used to confirm upconversion luminescent properties within the Vis spectrum of the Er^{+3} at room temperature with an ISS, PC1 Photon Counting Spectrofluorometer (PC1) operating in front surface mode. An excitation wavelength of 488 nm was filtered from a 300W high-pressure xenon arc lamp using a monochromator and the resultant emission spectrum was detected by a photomultiplier tube (Hamamatsu, R928) from 385 to 430 nm.

2.5. Photocatalytic testing

The photocatalytic activities were determined under UV, UV–vis, or IR irradiance using the photocatalyic degradation of rose bengal dye (RB) as the model reaction. Prior to conducting the experiments, adsorption studies were performed to determine the proper amount of RB to add to ensure a constant supernatant dye concentration after allowing equilibrium to be reached. The UV and UV–vis experiments were conducted using a batch slurry reactor and 5 fluorescent light bulbs enclosed in a light box impervious to ambient light. 8W, Rayonet RPR-3500 fluorescent 'blacklights' provided 315–400 nm light for the UV experiments while 8 W, General Electric F8T5/D fluorescent bulbs (Color Rendering Index 75) produced 60 W/m^2 of a 'daylight spectrum' for the UV–vis experiments. The intensity measurements for the 'daylight' bulbs were taken with a Li-Cor Paranometer Vis (400–1100 nm). Prior to turning on the light source, the catalyst and a predetermined amount of RB dye were allowed to reach equilibrium, resulting in an initial dye concentration (molar basis) of 200 ppb. A catalyst loading of 0.06 g TiO_2 was used and the initial volume of ultrapure water was 100 mL. This loading (0.6 g/L TiO_2) is consistent with the total solids loading of 1 g/L used in previous studies. [6,35] A further increase in loading (to 2 g/L for example [35]) led to decreased rates and could be caused by increased photon scattering and/or decreased photon penetration. [36]

Aliquots (1 mL) were removed every 60 s for UV experiments and every 5 min for UV–vis experiments while keeping the final volume removed below 10% of the initial reaction volume. UV–vis spectroscopy (Perkin Elmer, Lambda 35 UV–vis spectrometer) was used to measure the absorbance of 549 nm light by the RB dye in the removed aliquots which determined the RB concentrations for the individual trials. A trial with pure YAG was conducted under UV conditions to investigate any possible dye degradation offered by the Y-Al oxide and/or UV radiation. Selected experiments were also conducted with phenol as the surrogate molecule to assess the role of the potential dye sensitization mechanism on the results. Apparent quantum yields (Φ_{UV-vis}) were calculated using the experimentally determined degradation rates and photon flux as follows for UV–vis experiments:

$$\Phi_{UV-Vis} = \frac{R_{RB}\left[\frac{mol}{s}\right]}{J\left[\frac{mol}{m^2 * s}\right] * A\left[m^2\right]} * 100\%$$

where R_{RB} is the initial degradation rate of rose bengal (RB), J is photon flux and A is irradiated area. Ultrapure water (Direct-Q UV3 millipore) was used in all photocatalytic testing.

IR experiments were performed in a fabricated, stainless steel recirculating batch reactor upon which two, 800 mW Thorlabs M940L3 IR, high-powered LEDs (940 nm; Pmax = 1000 mW; FWHM = 37 nm), were mounted and provided 940 nm light (37 nm FWHM). Select experiments with other LEDS also described and include green (530 nm; Pmax = 370 mW; FWHM = 33 nm) and red (660 nm; Pmax = 700 mW; FWHM = 25 nm) LEDs. Photolysis was only measured for the green LEDs. The prepared composite was immobilized on a glass slide and given proper time reached equilibrium with the RB. The evolution of the characteristic 549 peak was again used to determine the RB concentration for individual trials. In order to properly investigate the sensitization enhancement offered by the addition of Yb^{+3} to the YAG:Er^{+3}, three additional YAG:Yb^{+3},Er^{+3} UP samples were synthesized and tested with a Yb^{+3} concentrations of 1, 2, and 3 mol%.

To inspect the reproducibility and stability, successive trials were also conducted in the recirculating batch reactor using the composite which performed the best in the UV–vis irradiation degradation experiments. Two 410 mW Thorlabs M405L2, high-powered UV (peak intensity at 405 nm) LEDs were used. During the final trial of the successive experiments, the pH (Denver Instruments pH meter) and the total organic carbon (Hach TOC kit) were used to compare the initial and final values.

3. Results and discussion

The composite catalysts and UPs are labeled with respect to the dopant amounts as denoted in Table 1. For all samples containing Er^{+3}, its concentration is 2 mol% in the host (YAG phase). To determine the effect of catalyst (TiO_2) to host (YAG) ratio, the ratio was altered and labeled as TiO_2/[x]YAG:Er^{+3} where x is the content in mol% of the YAG phase. Yb^{+3} was not included in this portion of the study. To determine the effect of Yb^{+3} doping into the YAG phase, the YAG amount relative to TiO_2 was maintained at 10 mol%. The Yb^{+3} in the host phase was altered and labeled as TiO_2/YAG:[y] Yb^{+3},Er^{+3} where y is the content in mol% of Yb^{+3} in the YAG phase.

3.1. Structural and morphological characterization of the UPs

The XRD patterns (Fig. 1) of the YAG:RE^{+3}indicated a well pronounced garnet phase ($Y_3Al_5O_{12}$) of the Y_2O_3-Al_2O_3 binary system remained after incorporation of the RE^{+3}. The diffraction lines corresponding to the (420), (211), and (400) indices retained their characteristic relative maximum intensities, confirming a well-developed YAG phase [37] as shown in Fig. 1(a). Diffraction lines at 2θ = 18, 29, 38 and 43° appeared in samples containing nominal mol% of $Yb^{+3} \geq 15\%$, which can be attributed to a small shift from the garnet phase to the monoclinic phase ($Y_4Al_2O_9$, YAM) [38] as shown in Fig. 1(b). A broadening of the (400) line is observed in the sample with Yb^{+3} amount of 10%, which indicated decreased crys-

Table 1
Labeling, dopant types and amounts and selected physical and optical properties of prepared TiO_2/YAG:RE^{+3} composites.

Sample label	Nominal content of RE^{+3} in YAG [mol%]	Nominal content of dopant [mol%]	YAG cell volume [nm^3][a]	Optical band gap, E_{bg} [eV][b]
TiO_2	–	–	–	3.02
YAG	–	–	1.74	–
TiO_2/YAG	–	10.0 YAG	1.74	–
TiO_2/[5]YAG:Er^{+3}	2.0 Er^{+3}	5.0 YAG:RE^{+3}	1.74	3.04
TiO_2/[10]YAG:Er^{+3}	2.0 Er^{+3}	10.0 YAG:RE^{+3}	1.74	3.04
TiO_2/[15]YAG:Er^{+3}	2.0 Er^{+3}	15.0 YAG:RE^{+3}	1.74	3.04
TiO_2/YAG:[10]Yb^{+3},Er^{+3}	10.0 Yb^{+3} 2.0 Er^{+3}	10.0 YAG:RE^{+3} 10.0 Yb^{+3}	1.77	3.04
TiO_2/YAG:[15]Yb^{+3},Er^{+3}	15.0 Yb^{+3} 2.0 Er^{+3}	10.0 YAG:RE^{+3} 15.0 Yb^{+3}	1.79	3.03
TiO_2/YAG:[20]Yb^{+3},Er^{+3}	20.0 Yb^{+3} 2.0 Er^{+3}	10.0 YAG:RE^{+3} 20.0 Yb^{+3}	1.80	3.03

[a] Determined from XRD, conducted on UPs before preparation into catalyst composite.
[b] Determined from DRS, conducted on catalyst composites.

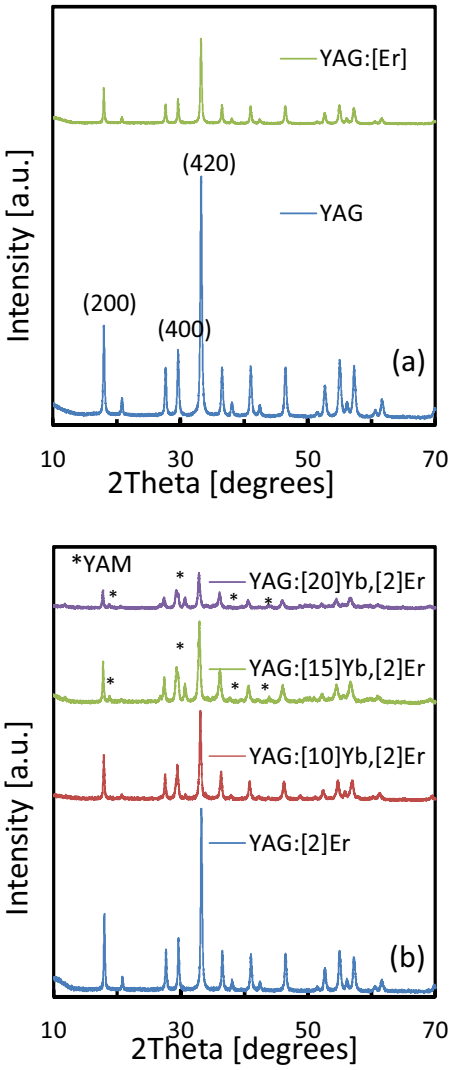

Fig. 1. (a) XRD of pure YAG and YAG:Er^{+3}. (b)XRD of selected YAG:RE^{+3} samples, with YAM diffraction lines labeled with (*) for YAG:[15,20]Yb^{+3},Er^{+3}.

tallite size. However, no clear evidence of YAM can be found in this sample. Er_2O_3 and Yb_2O_3 diffraction lines were not found in any of the YAG:RE^{+3} samples.

Correlating to the shifts of the diffractions lines of the YAG phase to lower angles, a noticeable increase in cell volume (see Table 1) can be seen with increasing amounts of Yb^{+3} which suggests that

Table 2
Chemical compositions of YAG:RE^{+3} UPs and TiO_2/YAG:RE^{+3} composite photocatalysts in atomic percent.

Sample/Element	% Ti	% O	% Y	% Al	% Er	% Yb
YAG	–	65.4	13.5	21.1	–	–
YAG:Er^{+3}	–	64.5	12.9	21.5	1.1	–
YAG:[10]Yb^{+3},Er^{+3}	–	62.1	12.9	20.0	0.8	4.2
YAG:[15]Yb^{+3},Er^{+3}	–	62.0	11.0	17.6	1.0	8.4
YAG:[20]Yb^{+3},Er^{+3}	–	59.0	15.5	10.5	1.2	13.8
TiO_2/YAG	23.4	66.6	3.9	6.1	–	–
TiO_2/YAG:Er^{+3}	25.8	66.1	3.0	4.7	0.4	–
TiO_2/YAG:[10]Yb^{+3},Er^{+3}	26.7	68.6	1.5	2.3	0.1	0.8
TiO_2/YAG:[15]Yb^{+3},Er^{+3}	26.9	67.6	1.6	2.8	0.1	1.0
TiO_2/YAG:[20]Yb^{+3},Er^{+3}	24.5	71.5	1.1	1.9	0.1	0.9

replacement of the smaller Al^{+3} (ionic radius = 0.535 Å) by larger Er^{+3} (ionic radius = 0.890 Å) and Yb^{+3} (ionic radius = 0.868 Å) is more likely to occur than replacement of Y^{+3} (ionic radius = 0.900 Å). The morphology and size distribution of the as-synthesized YAG:RE^{+3} were investigated by TEM. A selection of the TEM images is shown in Fig. 2, which displays how the UP maintained a polycrystalline appearance and particle size distribution of 30–90 nm. With increasing [Yb^{+3}], the large particles appear as similar size, but the average particle size increases.

3.2. Chemical composition analysis

The compositions of the UP and composite photocatalysts were determined by EDS and are reported in Table 2. Examination of the data revealed proper incorporation of the Er^{+3} at loading of 1.03+/− 0.17 atomic percent (at%) in the UPs and a doubling in Yb^{+3} amounts for the YAG:[10,15,20]Yb^{+3},Er^{+3} series of UPs. A noticeable decrease in Al and O compositions can be seen as assumed Yb^{+3} contents reach above 15 mol% which correlates well with what was found from XRD in that a phase shift from $Y_3Al_5O_{12}$ to $Y_4Al_2O_9$ was observed in these samples. Y content also peaked at the maximum Yb^{+3} loading, once again agreeing with the increase of Y:Al from 3:5 to 2:1 and Y:O from 1:4 to 4:9 resulting from a change in crystallinity. The data also confirmed that mixing the various UPs, which have varying molar masses, with titania resulted in a uniform Ti loading of 25.5+/− 1.5 at%. Confirmation of uniform Ti loading negated the possibility of altered rates due to comparison of composites with mixed compositions of photocatalyst, which would result in fluctuating amounts of active sites.

3.3. Optical characterization

Optical properties of the TiO_2/YAG:RE^{+3} composites were studied using DRS in the range of 350–1200 nm. In Fig. 3(a), relatively

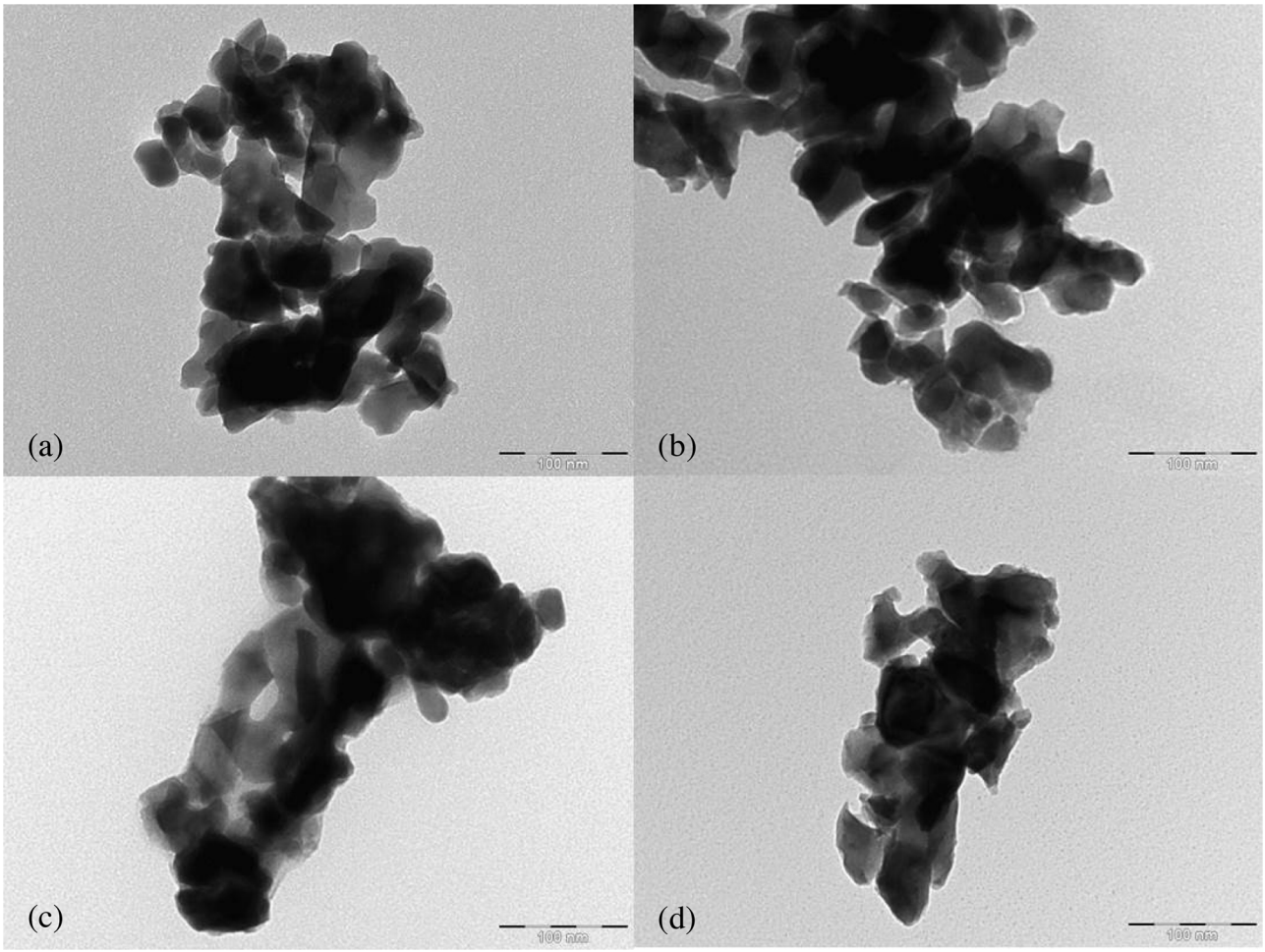

Fig. 2. Selected TEM images representing (a) YAG:Er, (b) YAG:[10]Yb,Er, (c) YAG:[15]Yb,Er and (d) YAG:[20]Yb,Er.

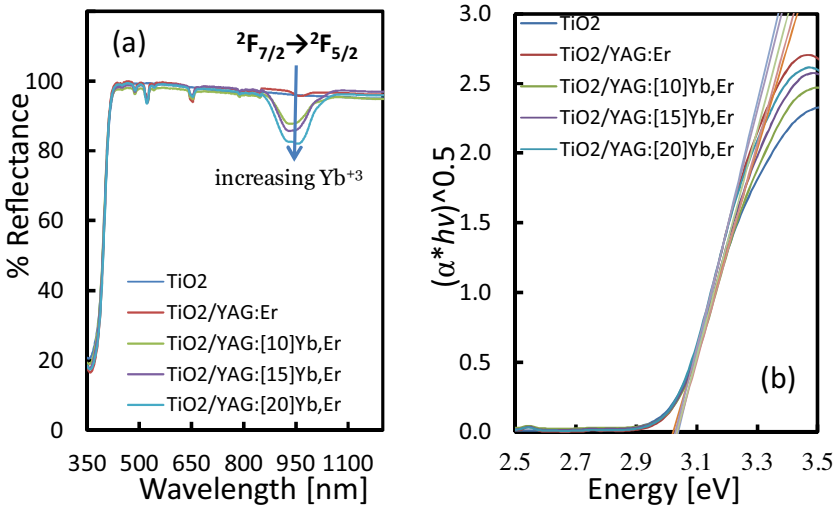

Fig. 3. (a) UV–vis-IR DRS of TiO_2/YAG:RE^{+3} composites with corresponding Yb^{+3} energy transition and (b) Tauc plot for optical band gap determination.

uniform reflectance peaks are seen throughout the Vis region which is expected due to a constant Er^{+3} concentration in all samples and Yb^{+3} lacking any activity throughout the Vis spectrum. Within the IR region, Er^{+3} contributions are only detectable in the TiO_2/YAG:Er^{+3} sample due to an overlap in reflectance peaks associated with Er^{+3} and Yb^{+3}. A broadening and intensification of the overlapping band correlating to the $^2F_{7/2} \rightarrow {}^2F_{5/2}$ energy transfer process of Yb^{+3} signifies successful incorporation of Yb^{+3} at increasing amounts [30]. Tauc plots of $(\alpha h\nu)^{0.5}$ vs. photon energy ($h\nu$) for the TiO_2/YAG:RE^{+3} composites are provided in Fig. 3(b) with TiO_2

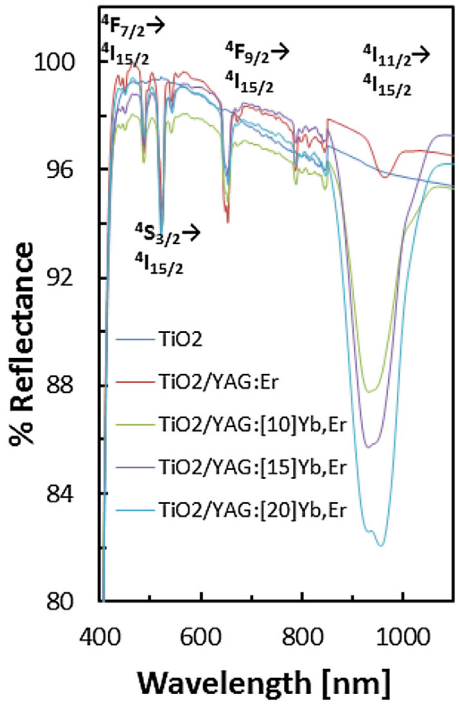

Fig. 4. UV–vis-IR DRS of TiO_2/YAG:RE composites with Er^{+3} energy transitions. Note that the Yb^{+3} transition labeled in the previous figure dominates the Er^{+3} transition near 900 nm.

as a reference material. The optical band gaps (E_{bg}) of the materials were estimated by using Tauc's formula:

$$(\alpha h\nu)^{\frac{2}{n}} = A\left(h\nu - E_{bg}\right)$$

where α is the absorption coefficient, n denotes the transition state (n = 4, indirect) and A is the slope of the tangent line corresponding to the point of inflection. The E_{bg} is found by locating the point of intersection on the x-axis of the tangent lines which are tabulated in Table 1. The addition of YAG:RE^{+3} does not have an effect on the E_{bg} of the titania photocatalyst which negates the possibility of improved or decreased reaction rates due to altering the fraction of light which has more energy than the associated E_{bg} for a given light source [1]. This being said, only photons with $E_p > 3.03$ eV (λ < 409 nm) have enough energy to initiate the photocatalytic process. Equivalent E_{bg} also allows for reliably comparing studies of UCL driven photocatalysis to be made in the absence of photons with $E_p > E_{bg}$ because the minimal required energy for each composite is the same. This is important because one of the intentions of this study is to gain insight into the applicability of intensified PL emissions of upconverted light due the sensitization of Er^{+3} by Yb^{+3} to a commercial titania photocatalyst. Given the nature of the RE^{+3}, ETU driven photocatalysis is restricted to light within the overlapping bands found in Fig. 3(a).

As shown in Fig. 4, the spectral bands throughout the Vis and IR regions associated with the absorption and scattering of light by Er^{+3} with peaks located at 488, 522, 654 and 968 nm. These bands are attributed to excitation from the Er^{+3} ground state $^4I_{15/2}$ to the excited states $^4F_{7/2}$, $^4S_{3/2}$, $^4F_{9/2}$, and $^4I_{11/2}$, respectively [29]. The significance of these bands is that they are located in the most intense region of the solar spectrum which allows for greater probability of upconversion luminescence to occur when solar radiation is used as the energetic light source for photocatalytic reactions [9]. The upconversion luminescence properties of RE^{+3} have been studied thoroughly over the last couple decades and low intensity UV emissions from Vis and IR excitation sources of Er^{+3} and Yb^{+3} doped/co-doped UP has been well documented

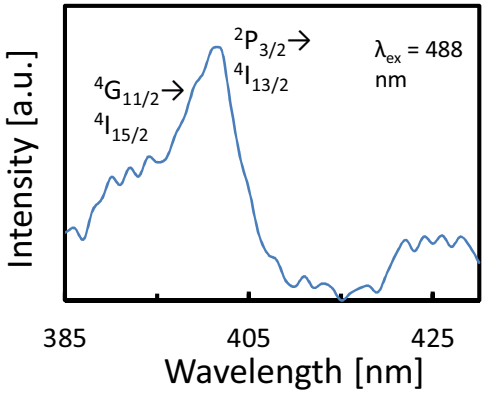

Fig. 5. PL spectrum of YAG:Er^{+3} resulting from 488 nm excitation.

[10,13,29,30]. The PL spectrum in Fig. 5 confirmed the generation of photons with $E_p > E_{bg}$ through Vis to UV upconversion luminescence by the YAG:Er^{+3} UP. The emission bands about 390 nm (3.18 eV) and 403 nm (4.07 eV) are attributed to the $^4G_{11/2} \rightarrow {}^4I_{15/2}$ and $^2P_{3/2} \rightarrow {}^4I_{13/2}$ transitions respectively and were obtained under 488 nm excitation [28].

3.4. Photocatalytic activity

RB dye has been reported to degrade primarily via hydroxyl radical attack, as opposes to direct oxidation or reduction of the dye due to a charge separation associated with an excited semiconductor molecule and is supported by various hydroxyl scavenger studies [32]. Control experiments confirmed negligible RB conversion in the absence of titania (~factor of 25 lower). However, dye sensitization pathway to RB photodegradation in the green light region cannot be excluded. This pathway is not anticipated to dominate over the photocatalytic pathway because of the lack of conversion in the photolysis control (no titania) experiment. For comparison, the control experiment (no catalyst) yielded RB conversion at a similar level compared to when titania was added when using green LEDs. The photon intensity in the green light region is over an order of magnitude higher for the LED than the broadband light, from which the insignificance of the dye sensitization pathway can be inferred.

All temporal profiles were consistent with pseudo-first order kinetics. Due to the first order dependence of the degradation rate on the model pollutant's concentration, it was important to maintain a constant initial supernatant dye concentration prior to activating the photocatalyst, which was achieved by conducting preliminary adsorption studies. In these studies, the adsorbed RB amount increased by ~10 micromoles/g TiO_2 (ranging from 9.8 to 12.7) when comparing the samples containing both TiO_2 and YAG versus just one of those components.

To determine the effect of the YAG:RE^{+3} content, a series of composites with 5, 10 and 15 mol% YAG:Er^{+3} were studied under UV–vis conditions resulting in a maximum initial degradation rate of −2.36 E-6 mol RB/(g*min) at 10 mol% (Fig. 6a). This correlates well with other findings which reported maximum degradation rates of titania/UP composites near a mass ratio of 1:1 [20], with the one from the present study being ~1:0.8. The decreased rate constant for the highest YAG:Er^{+3} amount compare to the optimal could be caused by RB adsorption on YAG too distance from the hydroxyl radicals generated by TiO_2 and/or blocking photon penetration into the slurry. The apparent quantum yields (Φ_{UV-vis}) are also reported in Table 3, which are typical of photocatalytic processes. Building upon these results, composites of varying Yb^{+3} amounts were subjected to the same UV–vis study with a YAG:RE^{+3}

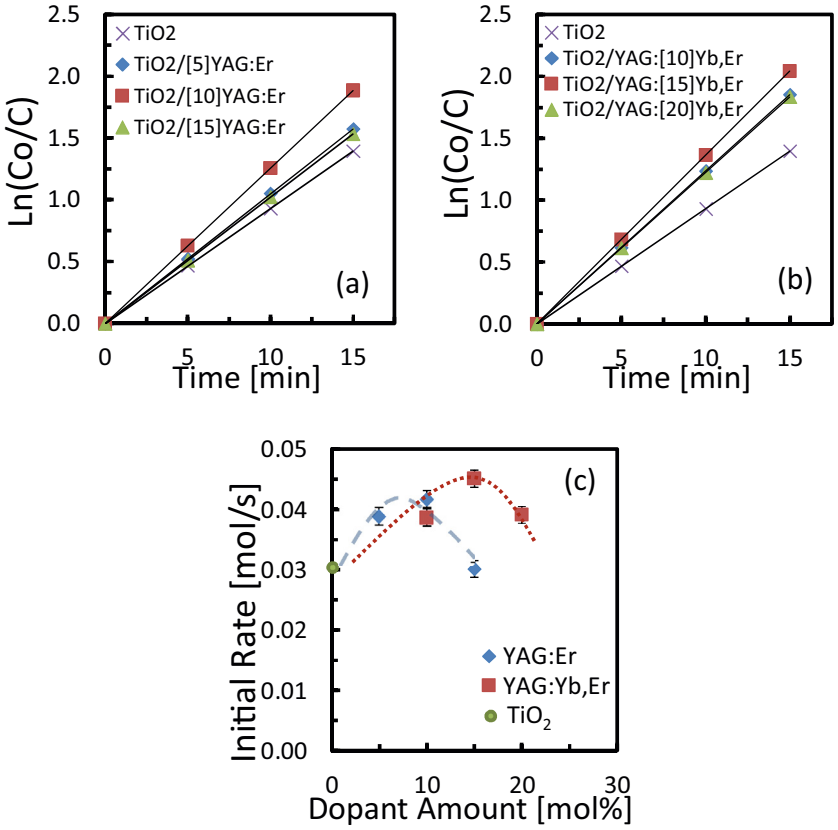

Fig. 6. RB degradation under UV–vis conditions in a slurry batch reactor for (a) TiO_2/[5,10,15]YAG:Er^{+3} and (b) TiO_2/YAG:[10,15,20]Yb^{+3},Er^{+3} composites. (c) Initial reaction rate as function of dopant concentration. In part (c), trend lines are provided to guide the reader.

Table 3
Rate constant (k'_{UV}) and Apparent Quantum Yields (Φ_{UV-vis}) of TiO_2/YAG:RE^{+3} photocatalysts for RB degradation under respective UV and UV–vis conditions.

Sample	k'_{UV} [mL/(g_{TiO2}*s)][a]	Φ_{UV-vis} [%][b]
TiO_2	9.42	0.0589
YAG	0.38	–
TiO_2/YAG	17.2	–
TiO_2/[5]YAG:Er^{+3}	–	0.0689
TiO_2/[10]YAG:Er^{+3}	18.3	0.0774
TiO_2/[15]YAG:Er^{+3}	–	0.0626
TiO_2/YAG:[10]Yb^{+3},Er^{+3}	–	0.0763
TiO_2/YAG:[15]Yb^{+3},Er^{+3}	20.7	0.0837
TiO_2/YAG:[20]Yb^{+3},Er^{+3}	–	0.0752

[a] Determined from UV initiated photocatalytic degradation in a slurry reactor.
[b] Determined from UV–vis initiated photocatalytic degradation in a slurry reactor. Average of three experiments is reported.

content of 10 mol%. Initially, the introduction of Yb^{+3} had a negative effect on the observed rate constant, reducing it by 3.1% at an Yb^{+3} amount of 10 mol% as seen in Table 3. However, when the Yb^{+3} content was raised from 10 to 15 mol% in the YAG:RE^{+3}, the degradation rate increased to −2.52 E-6 mol RB/(g*min) which is a 6.8% increase from that which was observed by the optimal YAG:Er^{+3} composite. Interestingly, the trend did not continue on to the next increase in Yb^{+3} content, which again had a negative effect on the TiO_2/[10]YAG:RE^{+3} ability to degrade the dye, but still improved upon bare P25 titania by 32%. The two separate progressions of varying contents of the host phase and Yb^{+3}, respectively, are displayed in Fig. 6(a) and (b), whereas the summary trends for the initial rates of the UV–vis studies as a function of dopants amounts are presented in Fig. 6(c). With the two optimized parameters (TiO_2/[10]YAG and YAG with [15]Yb^{+3},Er^{+3}), a 42% increase compared to TiO_2 P25 was observed in UV–vis light.

Since this increase is unlikely to occur from upconversion alone and literature has proposed dual enhancement mechanisms when the rare earth ion was embedded into the semiconductor [9,10,16], further investigations were conducted to dig deeper into the phenomena that have caused the enhancement. Since, in this study, the rare earth ions were not embedded into the semiconductor, the enhancements were unlikely to be caused by electronic effects which directly suppressed the recombination rates of e^-/h^+ pairs. However, there could be improved charge separation due to interfacial charge transfer in the composite system and increased organic adsorption. These effects could differ among the samples because of the varying compositions overall and of the components, but also due to the slight shift in crystalline phase of the Y_2O_3-Al_2O_3 binary system from garnet to monoclinic.

To investigate these possibilities, similar studies were conducted with bare P25 titania and the TiO_2/[10]YAG, TiO_2/[10]YAG:Er^{+3}, and TiO_2/YAG:[15]Yb^{+3},Er^{+3} composites under UV conditions. The reasoning behind these trials was to eliminate the role of upconversion, making the electronic effect on the suppressed e^-/h^+ recombination rates and the organic adsorption as the key parameters to impact the rate. The results (Fig. 7 and Table 3) once again indicated that the TiO_2/YAG:[15]Yb^{+3},Er^{+3} composite had the higher rate and rate constant (13.2% higher, as compared to 6.8% higher when in UV–vis light) than the similar catalyst without Yb. Compared to bare P25 titania, the TiO_2/[10]YAG:Er^{+3} and the TiO_2/YAG:[15]Yb^{+3},Er^{+3} samples improved the rate coefficient in UV light by 93% (compared to 31% in UV–vis light) and 120% (compared to 42% in UV–vis light), respectively.

These findings suggest that the enhancements measured during the UV–vis trials were dominated by electronic interactions of the titania photocatalyst and YAG:RE^{+3} and/or increased organic

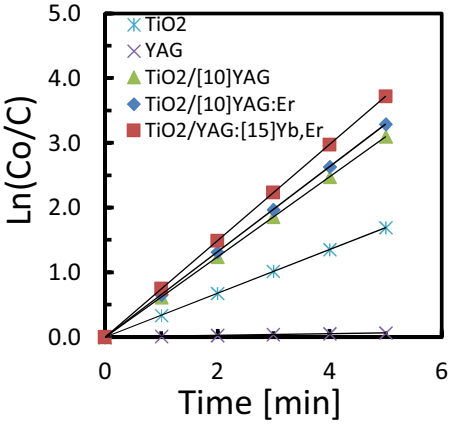

Fig. 7. RB degradation under UV conditions in a slurry batch reactor.

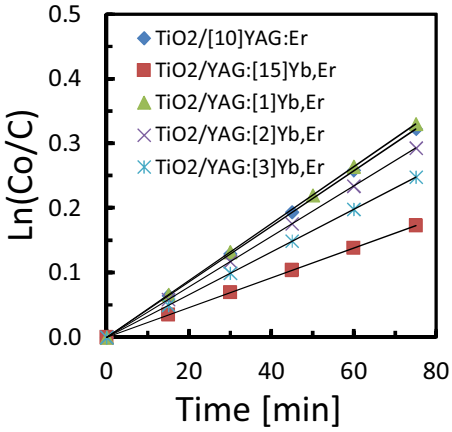

Fig. 8. RB degradation under IR conditions in a recirculating batch reactor.

adsorption. These claims are supported by the fact that the TiO_2/YAG enhanced the observed reaction rate coefficient by 83% when compared to pure titania even though no conversion was observed when pure YAG was tested alone. Since the P25 titania and the YAG have similar specific surface areas (~50 $m^2\,g^{-1}$ [22]) and titania:YAG mass ratio of 1:0.8 was used, it would be reasonable for the enhancements to be primarily caused by the increased organic adsorption as the hydroxyl radicals can travel to the adsorbed organics provided that there is intimate contact between the components. This conclusion is consistent with the increased RB adsorption (on a TiO_2 basis) prior to the photocatalysis (during dark equilibration) for the samples containing both TiO_2 and YAG rather than just TiO_2 or YAG. Alternatively, the interfacial charge transfer between phases is contributing to decreased charge carrier recombination rates. However, since YAG is a wide band gap semiconductor with the conduction band higher and valence band lower than those respective bands of TiO_2 [39,40], the scenario would be classified as "Included" (Type III [41]), meaning that both charge carriers would be expected to be transferred from YAG to TiO_2 if YAG could be excited. With the irradiation energy being too low to induce charge carriers in YAG due to its wide band gap, interfacial charge transfer would be expected to be minimal. As a result, increased organic adsorption is the most logical explanation for the improved performance. This explanation is also consistent with the samples' activity (increasing with increasing dopant amounts in the host phase) under UV irradiation correlating to decreasing crystallinity of the host phase with (Fig. 1b) and thus higher specific surface areas.

To cover all possible scenarios applicable to the TiO_2/YAG:RE^{+3} composite under solar radiation, further investigations were conducted using IR irradiation. A recirculating batch reactor was used in which only a fraction of the fluid was exposed to light while the remainder recirculated using a pump. The reactor vessel was equipped with two LEDs, which were IR ones with a spectrum centered at 940 nm with a bandwidth (FWHM) of 37 nm. Utilization of this light source improves upon sensitization studies intended to be applied to solar photocatalyst as it encompasses the entire overlapping spectra of the Yb^{+3} and Er^{+3} found from DRS rather than using a laser which supplies a narrower bandwidth. Normalization of the data also differed from the UV and UV–vis trials as the illuminated surface areas were used as a normalization factor opposed to the weight of titania present. This route was backed up by performing a thickness test of the immobilized films and it was found that additional layers of composite did not increase reaction rates due to the inability of photons to penetrate any further through the films, justifying normalization by surface area. Initially, a comparison was made between the TiO_2/[10]YAG:Er^{+3} and TiO_2/YAG:[15]Yb^{+3},Er^{+3} composites (Fig. 8 and Table 4) and the addition of Yb^{+3} was found to severely retard the degradation of RB dye. The explanation is that an overabundance of sensitizing ions resulted in self-quenching by cross-relaxation and cooperative UCL of neighboring excited Yb^{+3} rather than the desired nonradiative transfer of energy to ground state and excited Er^{+3} referred to as sensitization [11].

Table 4
Rate constant (k''_{IR}) of TiO_2/YAG:RE^{+3} photocatalysts for RB degradation under IR conditions.

Sample	k''_{IR} [mL/(cm^2*s)][a]
TiO_2/YAG:Er^{+3}	0.00581
TiO_2/YAG:[15]Yb^{+3},Er^{+3}	0.00311
TiO_2/YAG:[1]Yb^{+3},Er^{+3}	0.00594
TiO_2/YAG:[2]Yb^{+3},Er^{+3}	0.00527
TiO_2/YAG:[3]Yb^{+3},Er^{+3}	0.00446

[a] Determined from IR initiated photocatalytic degradation in a recirculating batch reactor. Rate coefficients are normalized to the area of photocatalyst film exposed to light.

To address this issue a separate series of composites were synthesized with Yb^{+3}:Er^{+3} of 05:1, 1:1 and 1.5:1 to be tested as previously reported [30] materials with low Yb^{+3}:Er^{+3} showed increased IR to Vis UCL emission. Even at low Yb^{+3}:Er^{+3}, increased degradation rates due to improved UV emissions from the addition of a sensitizing ion proves unlikely to occur. As seen in Fig. 8 and Table 4, the addition of 1 mol% Yb^{+3} does not effectively change the observed degradation rate and the addition of 2 mol% Yb^{+3} reduces the rate by 9%. These results seem to agree with what has been previously reported in regards to Yb^{+3}-Er^{+3} co-doped materials in that the sensitization of Er^{+3} by Yb^{+3} typically results in increased red and green UCL emissions and claims of improved IR to UV emissions have been limited to Tm^{+3}/Ho^{+3}-Yb^{+3} co-doped systems [13,19]. These results reinforced that the contribution of upconversion in the enhancements was overshadowed by other phenomena. The finding that the optimal composition of the photocatalyst differs for various photocatalytic mechanisms represents a significant practical challenge for effectively using all wavelengths of light. Since the enhancement from upconversion (IR conditions) is low compared to enhancements through formulation changed under UV and UV–vis conditions, the study suggests it is better to aim for improvements through those components rather than upconversion with IR photons.

In the next series of experiments, successive trials of the most active sample under UV–vis conditions (TiO_2/YAG:[15]Yb^{+3},Er^{+3}) was performed in the recirculating batch reactor which was now irradiated via two UV LEDs (centered at 405 nm). As shown in Fig. 9, the results indicated that the rate constant was stable over five suc-

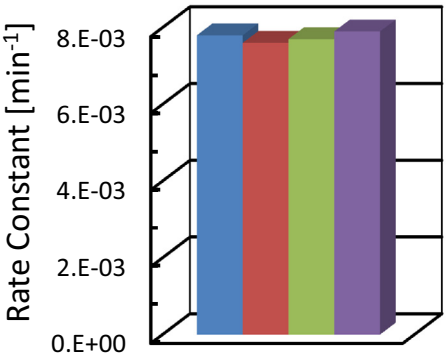

Fig. 9. RB degradation rate constant for the TiO_2/YAG:[15]Yb^{+3},Er^{+3} under UV conditions in recirculating batch reactor for four successive trials.

cessive degradation experiments. This finding was important as it verifies that the enhancement caused by improved dye adsorption was not limited to the first cycle. As a result, the increased rate coefficients are attributed to a reduction in the distance hydroxyl radicals, generated through the photocatalytic process, need to travel in order to degrade the organic dye. Diminished diffusion barriers are justified by both the successive trials and the pre-photocatalytic adsorption studies in that the adsorbed dye was not immobilized on the UP surface and in fact was destroyed and replaced by other dye molecules. In the final cycle of this experiment, the pH and TOC were analyzed. The pH decreased slightly, with a change from 6.63 to 6.23, which could be consistent with halides from RB now being free in solution. Another sign for complete degradation is that the decreases of TOC from initial to final closely match the conversion of RB.

In the final series of experiments, phenol was examined as a model pollutant using the slurry reactor described above with UV–vis conditions. The transient batch kinetic profiles again followed pseudo-first order kinetics. The P25 titania sample yielded a mass normalized rate constant of 0.067 mL $g_{TiO2}{}^{-1}$ s^{-1}, which is much lower than reported above for RB under UV conditions due to the much lower flux of UV photons in these experiments using simulated solar irradiation. The optimal formulation under these conditions yielded a mass normalized rate constant of 0.091 mL $g_{TiO2}{}^{-1}$ s^{-1}. This value represents a 36% increase compared to the P25 titania sample and is consistent with the 42% observed for RB degradation under similar conditions. This comparison validates the results as suitable for other degradation reactions and confirms that the RB dye sensitization mechanism is not a dominant contributor to the comparisons among samples.

4. Conclusions

A mixed phased, Y-Al oxide doped with 2 mol% Er^{+3} and 15 mol% Yb^{+3} was determined to yield the largest enhancement (42% increase) to a commercially available TiO_2 photocatalyst (P25) under simulated solar irradiation. Through selected control experiments and isolation of UV and IR contributions of solar irradiation, results suggested that increased pollutant adsorption near the photocatalysts' surface was the primary reason for the enhanced performances, as opposed to upconversion, decreased recombination rate of electron-hole pairs, or changes in band gap. This mechanism of enhancement coincided with a small phase shift from garnet to monoclinic in the Y-Al oxide structure, which unfortunately reduced UV emissions from UPs as shown from the IR experiments. The results of this study are useful as a third pathway for enhancement has been demonstrated, in addition to upconversion and decreased recombination rates.

Acknowledgements

Support from NSF grant EEC-1301054 is gratefully acknowledged. Partial support from the Office of Undergraduate Research at USF and the Florida Department of Agriculture and Consumer Services, Division of Aquaculture is also acknowledged. The authors thank Anne Meier for aiding in the SEM/EDS data collection and Daniel R. Russell for assistance with several photocatalysis experiments.

References

[1] S. Ahmed, M.G. Rasul, W.N. Martens, R. Brown, M.A. Hashi, Desalination 261 (2010) 3–18.
[2] M.R. Hoffmann, S.T. Martin, W.-I. Choi, D.W. Bahnemann, Chem. Rev. 95 (1995) 69–96.
[3] Y. Cho, W. Choi, C.-H. Lee, T. Hyeon, H.-I. Lee, Environ. Sci. Technol. 35 (2001) 966–970.
[4] A. Di Paola, G. Marcı', L. Palmisano, M. Schiavello, K. Uosaki, S. Ikeda, B. Ohtani, J. Phys. Chem. B 106 (2002) 637–645.
[5] P. Christopher, D.B. Ingram, S. Linic, J. Phys. Chem. C 114 (2010) 9173–9177.
[6] S.L. Pettit, C.H. McCane, J.T. Wolan, J.N. Kuhn, Catal. Lett. 43 (2013) 772–776.
[7] X. Jiang, Y. Wang, C. Pan, J. Alloys Compd. 509 (20) (2016) L137–L141.
[8] S. Obregón, G. Colón, Appl. Catal. B: Environ. 140–141 (2013) 299–305.
[9] S. Obregón, A. Kubacka, M. Fernández-García, G. Colón, J. Catal. 299 (2013) 298–306.
[10] J. Reszczynskaí, T. Grzyb, J.W. Sobczak, W. Lisowski, M. Gazda, B. Ohtani, A. Zaleska, Appl. Catal. B: Environ. 163 (2015) 40–49.
[11] F. Auzel, Chem. Rev. 104 (2004) 139.
[12] S. Han, R. Deng, X. Xie, X. Liu, Angew. Chem. Int. Ed. 53 (2014) 11702–11715.
[13] X. Wu, S. Yin, Q. Dong, B. Liu, Y. Wang, T. Sekino, S.W. Lee, T. Sato, Sci. Rep. 3 (2918) (2013) 1–8.
[14] Z. Zhang, W. Wang, W. Yin, M. Shang, L. Wang, S. Sun, Appl. Catal. B: Environ. 101 (2010) 68–73.
[15] W. Wang, M. Ding, C. Lu, Y. Ni, Z. Xu, Appl. Catal. B: Environ. 144 (2014) 379–385.
[16] S. Obregón, G. Colon, Appl. Catal. B: Environ. 158–159 (2014) 242.
[17] S. Obregón, S.W. Lee, G. Colon, Dalton Trans. 43 (2014) 311–316.
[18] J. Shi, J. Ye, L. Ma, S. Ouyang, D. Jing, L. Guo, Chem. Eur. J. 18 (2012) 7543–7551.
[19] X. Guo, W. Di, C.-H. Chen, C. Liu, X. Wang, W. Qin, Dalton Trans. 43 (2014) 1048–1054.
[20] G. Feng, S. Liu, Z. Xiu, Y. Zhang, J. Yu, Y. Chen, J. Phys. Chem. C 112 (2008) 13692–13699.
[21] L. Yin, Y. Li, J. Wanf, Y. Zhi, Y. Kong, Y. Gao, G. Han, P. Fan, J. Lumin. 132 (2012) 3010–3018.
[22] P. Lin, Q. Xiaoying, L. Di, Z. Jian, J. Rare Earth Met. 26 (2008) 674–677.
[23] Y. Ru, Q. Jie, L. Min, L. Guoqiang, J. Eur. Ceram. Soc. 28 (2008) 2903–2914.
[24] N. Zu, H. Yang, Z. Dai, Phys. B 403 (2008) 174–177.
[25] J. Silver, M.-I. Martinez-Rubio, T.G. Ireland, G.R. Fern, R. Withnall, J. Phys. Chem. B 105 (2001) 948–953.
[26] J. Silver, M.-I. Martinez-Rubio, T.G. Ireland, R. Withnall, J. Phys. Chem. B 105 (2001) 7200–7204.
[27] F. Gonnell, M. Haro, R.S. Sanchez, P. Negro, I. Mora-Sero, J. Bisquert, B. Juliaín-Loípez, S. Gimenez, J. Phys. Chem. C 118 (2014) 11279–11284.
[28] X. Wang, G. Shan, K. Chao, Y. Zhang, R. Liu, L. Feng, Q. Zeng, Y. Sun, Y. Liu, X. Kong, Mater. Chem. Phys. 99 (2006) 370–374.
[29] G. De, W. Qin, J. Zhang, J. Zhang, Y. Wang, C. Cao, Y. Cui, J. Lumin. 119–120 (2006) 258–263.
[30] F. Huang, X. Liu, Y. Ma, S.C. Kang, L. Hu, D. Chen, Sci. Rep. 5 (2015) 8233.
[31] R. Kumawat, I. Bhati, R. Ameta, Ind. J. Chem. Technol. 19 (2012) 191–194.
[32] S.B. Sharma, R. Ameta, R. Malkani, S. Ameta, J. Serb. Chem. Soc. 78 (2013) 897–905.
[33] N. Mittal, A. Shah, P.B. Punjabi, V.K. Sharma, Rasayan J. Chem. 2 (2009) 516–520.
[34] S.A. Hassanzadeh-Tabrizi, Adv. Powder Technol. 23 (2012) 324–327.
[35] J. Rashid, M.A. Barakat, S.L. Pettit, J.N. Kuhn, Environ. Technol. 35 (2014) 2153–2159.
[36] H. Kisch, D. Bahnemann, J. Phys. Chem. Lett. 6 (2015) 1907–1910.
[37] E. Garskaite, D. Jasaitis, A. Kareiva, J. Serb. Chem. Soc. 68 (2003) 677–684.
[38] P. Rai, M.-K. Song, H.-M. Song, J.-H. Kim, Y.-S. Kim, I.-H. Lee, Y.-T. Yu, Ceram. Int. 38 (2012) 235–242.
[39] J. Ueda, P. Dorenbos, A.J.J. Bos, K. Kuroishia, S. Tanabe, J. Mater. Chem. C 3 (2015) 5642–5651.
[40] V.P. Indrakanti, J.D. Kubicki, H.H. Schobert, Energy Environ. Sci. 2 (2009) 745–758.
[41] Y. Mi, Y. Weng, Sci. Rep. 5 (2015) 11482.